

Design of cost-efficient and photocatalytically active Zn-based MOFs decorated with Cu₂O nanoparticles for CO₂ methanation

Received 00th January 20xx,
Accepted 00th January 20xx

DOI: 10.1039/x0xx00000x

María Cabrero-Antonino,^{a,†} Sonia Remiro-Buenamañana,^{b,†} Manuel Souto,^c Antonio A. García-Valdivia,^d Duane Choquesillo-Lazarte,^e Sergio Navalón,^a Antonio Rodríguez-Diéguez,^{d,*} Guillermo Mínguez Espallargas,^{c,*} and Hemenegildo García^{a,b,*}

Here we show for the first time a MOF that is photocatalytically active for the light-assisted CO₂ methanation at mild conditions (215 °C) without the inclusion of metallic nanoparticles or any sacrificial agent. The presence of Cu₂O nanoparticles causes a 50 % increase in the photocatalytic activity. These results pave the way to developing efficient and cost-effective materials for CO₂ elimination.

The development of technologies that allow the efficient fixation and transformation of CO₂ into valuable chemicals such as CH₃OH, or fuels such as CH₄ will allow to decrease the atmosphere emissions of the main greenhouse gas responsible for global warming.¹ One of the traditional routes for this purpose is the Sabatier reaction, that consists in the CO₂ reduction to CH₄ using molecular H₂. This reaction occurs at high temperatures, typically above 550 °C, and requires the presence of a heterogeneous catalyst. In general, high efficiencies can be achieved employing noble metal nanoparticles (NPs) or clusters as active centres supported in high surface area materials.^{1,2} Some cost-effective metals such as Cu, Co or Ni can be employed as active centres for CO₂ methanation, although metal NP sintering commonly occurs at high temperatures (~300 °C) causing catalyst deactivation.^{2,3} More recently, the photocatalytic version of the Sabatier reaction is becoming a possible alternative, allowing to decrease the reaction temperature with a minimum impact on the resulting catalytic activity and partially avoiding catalyst deactivation by metal NPs aggregation.⁴

During the last 30 years, metal-organic frameworks (MOFs), materials constituted by organic ligands coordinated to metal ions or clusters defining a porous and crystalline

network,⁵ have been employed for the CO₂ fixation and/or valorisation.⁶ In addition, MOFs have shown to be excellent catalysts for different reactions,⁷ and are even currently used as photocatalysts,⁸ for visible light CO₂ reduction by triethanolamine,⁹ or for promoting C-C bond formation.¹⁰ In most of the cases, they exhibit an intrinsic photoresponse which can be combined with the presence of metal NPs in the pores in order to promote charge separation favouring the electron transfer to the substrate.¹¹ However, the use of MOFs to promote the Sabatier reaction is almost unexplored,^{12,13} possibly due to the severe conditions of this reaction that are not compatible with the stability of many MOFs.

In this work, we report the photoassisted CO₂ methanation by a MOF of formula [Zn₃(btca)₂(OH)₂] (H₂btca = 1,2,3-benzotriazole-5-carboxylic acid).¹⁴ This MOF, denoted as **MOF(Zn)-1**, is based on infinite rod-shape secondary building units (SBUs) formed by two independent 6-coordinated Zn(II) centres bridged by hydroxyl groups and by carboxylate and triazolate groups from the ligand (Fig. 1a). This flexible MOF contains 1D pores whose size depends on the degree of solvation (see ESI, Fig. S1 and S2). The CO₂ sorption capacity of **MOF(Zn)-1** has been previously described with different values depending on the activation temperature: Xiao *et al.*¹⁴ reported a BET surface area of 700 m²/g calculated from CO₂ sorption at 1 bar and 195 K when activating the material at 440 °C, whereas Yue *et al.*¹⁵ reported a BET value of 300 m²/g, under the same conditions, when the material was activated at 150 °C. In order to further understand these contradictory results, we have performed a detailed structural analysis on the different degree of breathing depending on the temperature of activation. We concluded that increasing the temperature causes a continuous breathing with a decrease in the volume cell similarly to other reported MOFs (see Fig. S1).¹⁶ However, upon further heating (above 400 °C), the MOF exhibits an irreversible phase transition with an unexpected pore opening and modification of the SBU and metal coordination environment, which is accompanied with some loss of crystallinity (see Fig. S2-S3). The activated sample at 400 °C is referred as **MOF(Zn)-2**.

MOF(Zn)-1 combines the presence of the active counterparts of the benchmark reference material for CO₂ methanation (ZnO), together with a N-electron rich heteroatom network of a porous structure with specific pore

^a Departamento de Química, Universitat Politècnica de València, c/Camino de Vera, s/n, 46022, Valencia, Spain.

^b Instituto de Tecnología Química (UPV-CSIC), Universitat Politècnica de València-CSIC, Av. De los Naranjos, 46022, Valencia, Spain

^c Instituto de Ciencia Molecular (ICMol), Universitat de València, c/Catedrático José Beltrán, 2, 46980 Paterna, Spain. E-mail: guillermo.minguez@uv.es.

^d Departamento de Química Inorgánica, Facultad de Ciencias, Universidad de Granada, 18071 Granada, Spain.

^e Laboratorio de Estudios Cristalográficos, IACT (CSIC-UGR), Avda. de las Palmeras 4, 18100, Armilla, Granada, Spain.

[†] Both contributors are considered as first authors.

Electronic Supplementary Information (ESI) available: General methods and materials, Structural features of MOF(Zn), Catalytic tests, Determination of valence band energies and optical gaps. CCDC numbers 1916082-1916087. See DOI: 10.1039/x0xx00000x

size for CO₂ interaction. Thus, we have explored the activity of this material for the photoassisted CO₂ methanation by molecular hydrogen, and compared it with **MOF(Zn)-2** and two reference materials, MOF-74(Zn),¹⁷ and MIL-125(Ti)-NH₂.¹⁸ MOF-74(Zn) is very similar to **MOF(Zn)-1** from a structural point of view, as both MOFs are formed by rod-like SBUs of the same metal (Zn^{II}), albeit in the case of MOF-74(Zn) with no nitrogenated ligands (Fig. 1b). MIL-125(Ti)-NH₂ exhibits a structure based on octameric Ti₈O₄(OH)₄ oxoclusters and 2-amino-terephthalate dianions, and has been shown to be an efficient photocatalyst.¹⁹

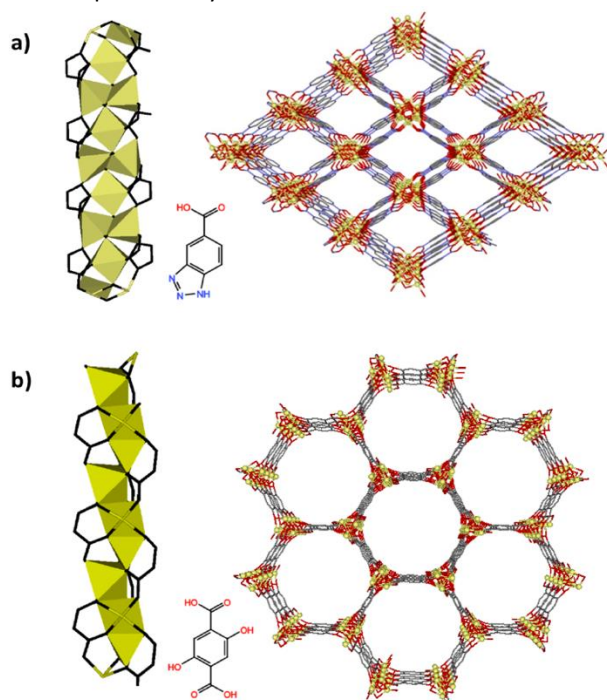


Fig. 1. Representation of crystal structures along *c*-axes of (a) **MOF(Zn)-1** and (b) MOF-74(Zn). The rod-like SBU is shown for each MOF, together with a schematic representation of the ligand.

MOF(Zn)-1 exhibits intrinsic activity for the selective photocatalytic CO₂ methanation under stoichiometric amount of hydrogen at 215 °C under UV-Vis irradiation (Fig. 2). The only product observed is methane, with an initial CH₄ production of 4 μmol·g_{cat}⁻¹·h⁻¹, and 30 μmol·g_{cat}⁻¹ after 24 hours. Although this activity value is not large, this is the first time that a bare MOF, i.e. without the addition of any nanoparticle or any sacrificial agent, exhibits photocatalytic activity for the Sabatier reaction. The temporal profile of CO₂ generation exhibits two regimes with two different reaction rates, which has been previously attributed to the effect of H₂O formed in the reaction simultaneously with CH₄ deactivating the catalyst.^{4c} Blank control experiments in the presence of the **MOF(Zn)-1** catalyst and H₂ as reducing agent but in the absence of CO₂, do not show the formation of methane. Similarly, performing the photocatalytic reaction at room temperature, or upon irradiation of visible light only, does not produce any methane. Other blank control in the absence of UV-Vis light irradiation results in a methane production lower than 0.1 μmol·g_{cat}⁻¹ after 24 h. Importantly,

the catalytic activity of MOF-74(Zn) or MIL-125(Ti)-NH₂ is negligible under the same reaction conditions (see Fig. 2). This lack of photocatalytic activity can be a consequence of the low harnessing ability of these MOFs in comparison to **MOF(Zn)-1**, as their CO₂ adsorption capacity is higher. Interestingly, **MOF(Zn)-2**, which has a wider pore aperture than **MOF(Zn)-1**, is less active (initial production of 2.88 μmol·g_{cat}⁻¹·h⁻¹ and 15 μmol·g_{cat}⁻¹ after 24 hours) for the photocatalytic CO₂ methanation than **MOF(Zn)-1**, which can be explained by the modification of the SBU and the loss in crystallinity of the bulk material upon temperature treatment, as shown by X-ray powder diffraction (see Fig. S2).

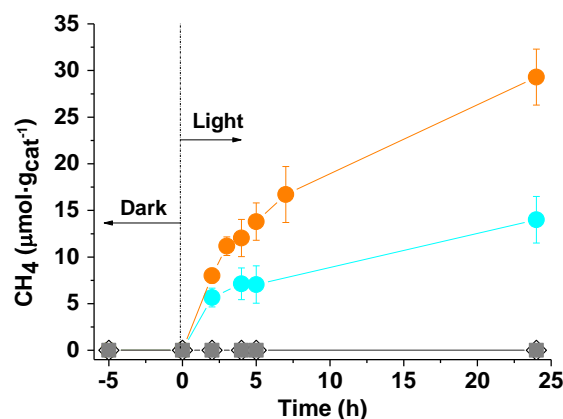


Fig. 2. CH₄ production obtained at 215 °C upon 2236 W·m⁻² irradiation using a 300 W Xe lamp. P_{H₂} = 1.05 bar, P_{CO₂} = 0.25 bar. **MOF(Zn)-1** (●), **MOF(Zn)-2** (●), MOF-74(Zn) (■), MIL-125(Ti)-NH₂ (◇).

In order to enhance the catalytic activity of **MOF(Zn)-1**, we have evaluated the influence of metal NPs in the pores of the MOF. Recently, Ni NPs encapsulated into the cavities of MIL-101(Cr) have resulted in a stable catalyst for the CO₂ methanation.¹² However, Cu NPs supported on ZnO finely dispersed in the high surface area Al₂O₃ support is a reference industrial material for CO₂ hydrogenation,²⁰ and it has been previously shown that Cu₂O is an active semiconductor for the photocatalytic CO₂ methanation.^{4b} Based on these precedents, we have prepared Cu₂O NPs deposited into **MOF(Zn)-1** by using the photodeposition method. For comparison, Cu₂O NPs were also deposited into **MOF(Zn)-2**, MOF-74(Zn) and MIL-125(Ti)-NH₂ solids.

Specifically, upon UV-Vis irradiation of a MOF suspension in an aqueous Cu²⁺ solution using methanol as sacrificial electron donor, Cu₂O NPs of few nm could be prepared. ICP-OES analyses confirm a ~1 wt% copper loading on the various MOFs. Powder X-ray diffraction (PXRD) measurements of the copper-supported MOFs confirm the stability of the materials during the photodeposition method while no peaks attributable to the diffraction of any copper species could be observed. This failure to detect Cu diffraction peaks can be attributed to the good dispersion of small copper NPs in the MOFs and/or low copper content of the catalysts (1 wt%). In agreement with this hypothesis, TEM analysis reveals that the narrowest copper particle size distribution is achieved using

MOF(Zn)-1 support (1.61 ± 0.46 nm), followed by MIL-125(Ti)-NH₂ (4.29 ± 0.95 nm), **MOF(Zn)-2** (5.35 ± 2.36 nm) and MOF-74(Zn) (6.07 ± 1.52 nm) (Fig. S4-S6). The small copper particle size achieved in the Cu₂O@**MOF(Zn)-1** is compatible with the internal location inside the pores. SEM measurements show that the morphology of **MOF(Zn)-1** or **MOF(Zn)-2** are not modified after copper deposition (Fig. S7) and copper NPs are well-dispersed in the MOFs (Fig. S8-S9).

XPS spectra of Cu₂O@**MOF(Zn)-1** and Cu₂O@**MOF(Zn)-2** reveal the presence of the different elements (C, O, N, Zn and Cu) in the samples (Fig. S9-S11). Regarding the high resolution XPS spectrum of Cu2p peak (Fig. S9d), the presence of Cu₂p_{3/2} and Cu₂p_{1/2} and their deconvolution allows to detect reduced copper species (Cu⁰ and/or Cu⁺) together with Cu²⁺. It should be noted, however, that under the photocatalytic reaction conditions at 215 °C under H₂ flow, the Cu²⁺ would be probably reduced to Cu⁺,²¹ while the reduction of Cu₂O to metallic copper starts to take place at temperatures above 300 °C.

The copper-containing MOF samples were evaluated as photocatalysts in the same conditions as pristine MOFs lacking Cu₂O nanoparticles (*vide supra*). The temporal evolution of CH₄ formation is presented in Fig. 3, which shows, as expected, an enhanced activity upon Cu₂O incorporation. As in the case of **MOF(Zn)-1**, the photocatalytic activity of Cu₂O@**MOF(Zn)-1** derives exclusively from the UV region. The deposition of copper NPs in MOF-74(Zn) and MIL-125(Ti)-NH₂ results in the formation of solids capable of promoting the CO₂ photoreduction by H₂ to CH₄, although it can be clearly observed that the best performing MOF photocatalyst is Cu₂O@**MOF(Zn)-1** (initial CH₄ production of 10 μmol·g_{cat}⁻¹·h⁻¹ and 45 μmol·g_{cat}⁻¹ after 24 hours), which increased around 50% its photocatalytic activity compared with the pristine MOF lacking Cu₂O particles. The estimated TOF of Cu₂O@**MOF(Zn)-1**, measured at 2 h after subtracting the activity of **MOF(Zn)-1**, is as high as about $50 \cdot 10^{-3}$ s⁻¹ at 215 °C, which is much better than reported for Ni@MIL-101(Cr) ($1.63 \cdot 10^{-3}$ s⁻¹ at 300 °C).¹²

To confirm the origin of methane, an additional experiment using ¹³C¹⁸O₂ as reagent was performed and the photoproduct analysed by GC-MS (Fig. S15), observing the formation of ¹³CH₄ (m/z 17) and H₂¹⁸O (m/z 20), accompanied by H₂¹⁶O (m/z 18), thus corroborating the simultaneous formation of CH₄ and H₂O.

The PXRD patterns of the used samples show that the MOF materials employed in this study retain their initial crystallinity under the present reaction conditions (Fig. S12). For the most active sample, Cu₂O@**MOF(Zn)-1**, TEM measurements of the used sample (Fig. S13) show that the average copper particle size distribution and standard deviation remain constant (1.7 ± 0.9 nm) respect to the fresh sample (1.6 ± 0.5 nm), and ICP-OES analysis of the used sample reveals that the copper content is practically the same than the fresh sample.

In fact, although Cu₂O exhibits intrinsic photocatalytic activity in the absence of support, the main limitation of this semiconductor is the stability under photocatalytic conditions,²² which is enhanced upon incorporation into the pores of **MOF(Zn)-1**, as previously demonstrated.²³

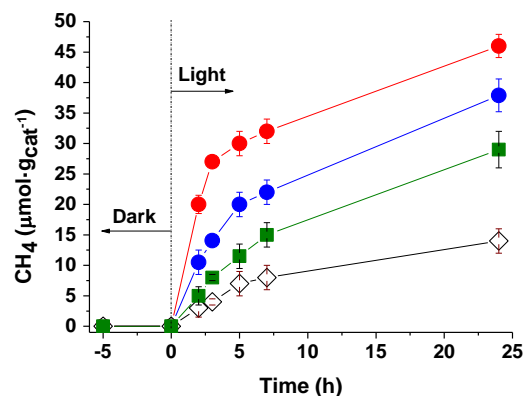


Fig. 3. CH₄ production using Cu₂O@MOFs working 215 °C upon 2236 W m⁻² irradiation using a 300 W Xe lamp. P_{H₂} = 1.05 bar, P_{CO₂} = 0.25 bar. Legend Cu₂O@**MOF(Zn)-1** (●), Cu₂O@**MOF(Zn)-2** (●), Cu₂O@MOF-74(Zn) (■), and Cu₂O@MIL-125(Ti)-NH₂ (◇).

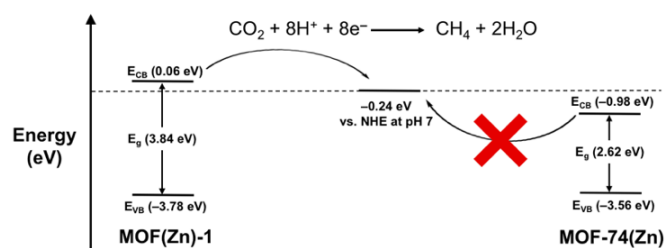


Fig. 4. Energetic diagram for **MOF(Zn)-1** and MOF-74(Zn). E_g has been calculated from the TAUC plot; E_{VB} calculated from the oxidation potential; and E_{CB} has been calculated from the following equation: E_{CB} = E_g + E_{VB} (see Fig. S16-S17 for details).

The higher activity of Cu₂O@**MOF(Zn)-1** is attributed to the intrinsic photoactivity of the material. This is revealed by self-activity of the support and, more importantly, further combination with small Cu₂O NPs behaving both as semiconductor and co-catalyst close to the Zn-O reduction centres. In addition, we have examined if the presence of incorporated Cu₂O NPs increase the charge separation efficiency. The lack of significant changes in the photoluminescence of **MOF(Zn)-1** in the absence and in the presence of occluded Cu₂O NPs suggests that there is no charge transfer between the two components, indicating that the charge recombination in **MOF(Zn)-1** is not altered by the presence of Cu₂O. The differences in photoactivity between **MOF(Zn)-1** and MOF-74(Zn) is further explained by the energy of the conduction of valence band, which has been experimentally determined by combination of electrochemistry (Fig. S16) and optical spectroscopy (Fig. S17). As can be seen in Fig. 4, the valence band energies are similar in both materials, but the optical band gaps (calculated from the absorption spectra) are remarkably different resulting in a different energy for the conduction bands (0.06 eV vs. -0.975 eV for **MOF(Zn)-1** and MOF-74(Zn) respectively). In fact, in the case of MOF-74(Zn), the conduction band energy is not enough to promote the photochemical reduction of CO₂ (-0.24 eV).²⁴ However, this process is thermodynamically possible in the case of **MOF(Zn)-1**, explaining why this material has intrinsic photocatalytic activity.

In summary, the photocatalytic activity for the light-assisted CO₂ methanation has been shown for the first time using a bare MOF, a Zn-based MOF denoted **MOF(Zn)-1**. The low temperature photocatalytic activity (215 °C) allows the use of MOFs in this important reaction, which is typically limited due to degradation caused by the extreme conditions (T > 500 °C). Furthermore, its activity has been additionally increased upon incorporation of small Cu₂O nanoparticles, with a TOF value of 50·10⁻³ s⁻¹ at 215 °C, the highest ever reported for a MOF. This result is the combination of a high intrusive photocatalytic activity of the framework with the small Cu₂O nanoparticles as co-catalyst. This work highlights the potential of specific MOF design to develop efficient and cost-effective materials to overcome the drawbacks derived from the increasing presence of the undesirable CO₂ greenhouse gas.

This work has been supported by the European Union (ERC-2016-CoG 724681-S-CAGE), the Spanish MICINN (Structures of Excellence María de Maeztu MDM-2015-0538 and Severo Ochoa SEV-2016-0683; projects CTQ2017-89528-P, CTQ2015-69163-CO2-R1 and PGC2018-102052-B-C21), Generalitat Valenciana (Prometeo 2017-083) and Junta de Andalucía (P12-FQM-1484). G.M.E. and M.S. thank MICINN for a “Ramón y Cajal” and a “Juan de la Cierva-Formación” fellowships, respectively. S.R.-B. thanks the Research Executive Agency (REA) and the European Commission for a Marie Skłodowska Curie fellowship (H2020-MSCA-IF-2015/Grant agreement number 709023/ZESMO). S.N. thanks the Fundación Ramón Areces (XVIII Concurso Nacional para la Adjudicación de Ayudas a la Investigación en Ciencias de la Vida y de la Materia, 2016).

Conflicts of interest

There are no conflicts to declare.

Notes and references

- a) X. Li, J. Yu, M. Jaroniec, and X. Chen, *Chem. Rev.* 2019, **119**, 3962; b) T. Sakakura, J.-C. Choi and H. Yasuda, *Chem. Rev.* 2007, **107**, 2365.
- M. Younas, L. L. Kong, M. J. K. Bashir, H. Nadeem, A. Shehzad and S. Sethupathi, *Energy Fuels*, 2016, **30**, 8815.
- S. Rönsch, J. Schneider, S. Matthischke, M. Schlüter, M. Götz, J. Lefebvre, P. Prabhakaran and S. Bajohr, *Fuel*, 2016, **166**, 276.
- a) T. Yui, A. Kan, C. Saitoh, K. Koike, T. Ibusuki and O. Ishitani, *ACS Appl. Mater. Interfaces*, 2011, **3**, 2594; b) D. Mateo, J. Albero and H. García, *Energy Environ. Sci.*, 2017, **10**, 2392; c) D. Mateo, D. De Masi, J. Albero, L.-M. Lacroix, P.-F. Fazzini, B. Chaudret and H. García, *Chem. Eur. J.*, 2018, **24**, 18436; d) D. Mateo, J. Albero and H. García, *Appl. Catal. B*, 2018, **224**, 563.
- a) H.-C. Zhou, J. R. Long and O. M. Yaghi, *Chem. Rev.* 2012, **112**, 673; b) G. Maurin, C. Serre, A. Cooper and G. Férey, *Chem. Soc. Rev.*, 2017, **46**, 3104.
- C. A. Trickett, A. Helal, B. A. Al-Maythaly, Z. H. Yamani, K. E. Cordova and O. M. Yaghi, *Nat. Rev. Mater.*, 2017, **2**, 17045.
- a) S. M. J. Rogge, *et al.*, *Chem. Soc. Rev.*, 2017, **46**, 3134; b) M. Souto, A. Santiago-Portillo, M. Palomino, I. J. Vitórica-Yrezábal, C. Vieira, J. C. Waerenborgh, S. Valencia, S. Navalón, H. García and G. Mínguez Espallargas, *Chem. Sci.*, 2018, **9**, 2413.
- a) Y. Li, H. Xu, S. Ouyang and J. Ye, *Phys. Chem. Chem. Phys.*, 2016, **18**, 7563; b) A. Dhakshinamoorthy, Z. Li and H. García, *Chem. Soc. Rev.*, 2018, **47**, 8134; c) R. Li, W. Zhang and K. Zhou, *Adv. Mater.*, 2018, **30**, 1705512; d) Y. Han, H. Xu, Y. Su, Z. Xu, K. Wang and W. Wang, *J. Catal.*, 2019, **370**, 70.
- a) D. Sun, Y. Gao, J. Fu, X. Zeng, Z. Chen and Z. Li, *Chem. Commun.*, 2015, **51**, 2645; b) Y. Lee, S. Kim, J. K. Kang and S. M. Cohen, *Chem. Commun.*, 2015, **51**, 5735.
- D. Shi, C. He, W. Sun, Z. Ming, C. Meng and C. Duan, *Chem. Commun.*, 2016, **52**, 4714.
- a) A. Dhakshinamoorthy, A. M. Asiri, and H. García, *Angew. Chem. Int. Ed.*, 2016, **55**, 5414; b) T. Zhang, Y. Jin, Y. Shi, M. Li, J. Li, and C. Duan, *Coord. Chem. Rev.*, 2019, **380**, 201; c) R. Li, W. Zhang and K. Zhou, *Adv. Mater.*, 2018, **30**, 1705512.
- W. Zhen, F. Gao, B. Tian, P. Ding, Y. Deng, Z. Li, H. Gao and G. Lu, *J. Catal.*, 2017, **348**, 200.
- a) M. Mon et al., *Angew. Chem. Int. Ed.*, 2018, **57**, 6186; b) Z.-W. Zhao, X. Zhou, Y.-N. Liu, C.-C. Shen, C.-Z. Yuan, Y. F. Jiang, S.-J. Zhao, L.-B. Ma, T.-Y. Cheang and Z.-W. Xu, *Catal. Sci. Technol.*, 2018, **8**, 3160; c) W. Zhen, B. Li, G. Lu and J. Ma, *Chem. Commun.*, 2015, **51**, 1728; d) R. Lippi et al., *J. Mater. Chem. A*, 2017, **5**, 12990.
- J. Xiao, Y. Wu, M. Li, B.-Y. Liu, X.-C. Huang and D. Li, *Chem. Eur. J.*, 2013, **19**, 1891.
- Y. Yue et al. *J. Phys. Chem. C*, 2015, **119**, 9442.
- a) G. Férey, C. Mellot-Draznieks, C. Serre, F. Millange, J. Dutour, S. Surblé and I. Margiolaki, *Science*, 2005, **309**, 2040; b) E. J. Carrington, C. A. McAnally, A. J. Fletcher, S. P. Thompson, M. Warren and L. Brammer, *Nat. Chem.*, 2017, **9**, 882; c) M. Souto, J. Romero, J. Calbo, I. J. Vitórica-Yrezábal, J. L. Zafra, J. Casado, E. Ortí, A. Walsh and G. Mínguez Espallargas, *J. Am. Chem. Soc.*, 2018, **140**, 10562.
- N. Rosi, J. Kim, M. Eddaoudi, B. Chen, M. O’Keeffe and O. M. Yaghi, *J. Am. Chem. Soc.*, 2005, **127**, 1504.
- a) M. Dan-Hardi, C. Serre, T. Frot, L. Rozes, G. Maurin, C. Sánchez and G. Férey, *J. Am. Chem. Soc.*, 2009, **131**, 10857; b) S. Vaesen et al., *Chem. Commun.*, 2013, **49**, 10082.
- a) Y. Yoshida and Y. Izumi, *J. Catal.*, 2015, **332**, 1; b) K. Meyer, S. Bashir, J. Llorca, H. Idriss, M. Ranocchiaro and J. A. van Bokhoven, *Chem. Eur. J.*, 2016, **22**, 13894; c) M. B. Chambers, *J. Am. Chem. Soc.*, 2017, **139**, 8222; d) S. Kampouri, T. N. Nguyen, M. Spodaryk, R. G. Palgrave, A. Züttel, B. Smit, K. C. and K. C. Stylianou, *Adv. Funct. Mater.*, 2018, **28**, 1806368.
- W. Wang, S. Wang, X. Ma and J. Gong, *Chem. Soc. Rev.*, 2011, **40**, 3703.
- J. Y. Kim, J. A. Rodriguez, J. C. Hanson, A. I. Frenkel and P. L. Lee, *J. Am. Chem. Soc.*, 2003, **125**, 10684.
- A. D. Handoko, J. Tiang, *Int. J. Hydrog. Energy*, 2013, **38**, 13017.
- a) M. Meilikhov, K. Yusenko, D. Esken, S. Turner, G. Van Tendeloo, R. A. Fischer, *Eur. J. Inorg. Chem.*, 2010, 3701; b) A. Santiago-Portillo, M. Cabrero-Antonino, M. Álvaro, S. Navalón, H. García, *Chem. Eur. J.*, 2019, **25**, 9280.
- S. N. Habisreutinger, L. Schmidt-Mende and J. K. Stolarczyk, *Angew. Chem. Int. Ed.*, 2013, **52**, 7372.